Specific disruption of thalamic inputs to the auditory cortex in schizophrenia models

Sungkun Chun *et al.*

Science **344**, 1178 (2014);
DOI: 10.1126/science.1253895

could promote branch-specific formation (Fig. 2D). Thus, it appears that which set of dendritic branches forms new spines is determined by specific features (input or activity patterns) of a learning task, rather than by sleep. Our data suggest that reactivation of task-specific neurons during NREM sleep is involved in forming new synapses after learning, although definitive proof that reactivation causes synaptic formation would require simultaneous imaging of both reactivation and synapses in the same neurons over time. Neuronal reactivation during sleep may promote branch-specific spine formation in a manner similar to awake learning experiences (Fig. 2D), and its effectiveness in promoting spine formation may vary at different times of the day (fig. S8). Sleep reactivation could also allow the expression of specific genes critical for the growth of new synaptic connections (*32*, *33*). Future studies are needed to address these questions in order to better understand how sleep contributes to memory storage in the brain.

REFERENCES AND NOTES

1. P. Maquet, *Science* **294**, 1048–1052 (2001).
2. J. M. Siegel, *Nature* **437**, 1264–1271 (2005).
3. R. Stickgold, *Nature* **437**, 1272–1278 (2005).
4. S. Diekelmann, J. Born, *Nat. Rev. Neurosci.* **11**, 114–126 (2010).
5. J. H. Benington, M. G. Frank, *Prog. Neurobiol.* **69**, 71–101 (2003).
6. C. Pavlides, J. Winson, *J. Neurosci.* **9**, 2907–2918 (1989).
7. W. E. Skaggs, B. L. McNaughton, *Science* **271**, 1870–1873 (1996).
8. A. S. Dave, D. Margoliash, *Science* **290**, 812–816 (2000).
9. M. A. Wilson, B. L. McNaughton, *Science* **265**, 676–679 (1994).
10. D. Ji, M. A. Wilson, *Nat. Neurosci.* **10**, 100–107 (2007).
11. S. Ribeiro *et al.*, *PLOS Biol.* **2**, E24 (2004).
12. A. S. Dave, A. C. Yu, D. Margoliash, *Science* **282**, 2250–2254 (1998).
13. R. R. Llinás, M. Steriade, *J. Neurophysiol.* **95**, 3297–3308 (2006).
14. V. Crunelli, S. W. Hughes, *Nat. Neurosci.* **13**, 9–17 (2010).
15. C. H. Bailey, E. R. Kandel, *Annu. Rev. Physiol.* **55**, 397–426 (1993).
16. J. W. Lichtman, H. Colman, *Neuron* **25**, 269–278 (2000).
17. D. H. Bhatt, S. Zhang, W. B. Gan, *Annu. Rev. Physiol.* **71**, 261–282 (2009).
18. G. Yang, F. Pan, W. B. Gan, *Nature* **462**, 920–924 (2009).
19. I. Timofeev, *Prog. Brain Res.* **193**, 121–144 (2011).
20. G. Wang, B. Grone, D. Colas, L. Appelbaum, P. Mourrain, *Trends Neurosci.* **34**, 452–463 (2011).
21. M. G. Frank, *Neural Plast.* **2012**, 264378 (2012).
22. J. Born, G. B. Feld, *Neuron* **75**, 933–935 (2012).
23. C. Cirelli, G. Tononi, *Ann. Med.* **31**, 117–124 (1999).
24. V. V. Vyazovskiy, C. Cirelli, M. Pfister-Genskow, U. Faraguna, G. Tononi, *Nat. Neurosci.* **11**, 200–208 (2008).
25. S. Maret, U. Faraguna, A. B. Nelson, C. Cirelli, G. Tononi, *Nat. Neurosci.* **14**, 1418–1420 (2011).
26. G. Yang, W. B. Gan, *Dev. Neurobiol.* **72**, 1391–1398 (2012).
27. J. M. Donlea, N. Ramanan, P. J. Shaw, *Science* **324**, 105–108 (2009).
28. D. Bushey, G. Tononi, C. Cirelli, *Science* **332**, 1576–1581 (2011).
29. G. Tononi, C. Cirelli, *Brain Res. Bull.* **62**, 143–150 (2003).
30. M. G. Frank, N. P. Issa, M. P. Stryker, *Neuron* **30**, 275–287 (2001).
31. S. Chauvette, J. Seigneur, I. Timofeev, *Neuron* **75**, 1105–1113 (2012).
32. S. J. Aton *et al.*, *Neuron* **61**, 454–466 (2009).
33. J. Seibt *et al.*, *Curr. Biol.* **22**, 676–682 (2012).
34. H. P. Roffwarg, J. N. Muzio, W. C. Dement, *Science* **152**, 604–619 (1966).
35. D. Jouvet-Mounier, L. Astic, D. Lacote, *Dev. Psychobiol.* **2**, 216–239 (1969).
36. C. Liston *et al.*, *Nat. Neurosci.* **16**, 698–705 (2013).
37. G. Yang, F. Pan, P. C. Chang, F. Gooden, W. B. Gan, *Methods Mol. Biol.* **1010**, 35–43 (2013).
38. P. V. Zelenin *et al.*, *J. Neurophysiol.* **105**, 2698–2714 (2011).
39. T. W. Chen *et al.*, *Nature* **499**, 295–300 (2013).
40. I. G. Campbell, I. Feinberg, *J. Neurophysiol.* **76**, 3714–3720 (1996).

ACKNOWLEDGMENTS

We thank all the members in the Gan laboratory and T. Franke for comments on the manuscript. This work was supported by NIH R01 NS047325 and P01 NS074972 to W.-B.G. and by a Whitehall Foundation research grant and an American Federation for Aging Research grant to G.Y.

SUPPLEMENTARY MATERIALS

www.sciencemag.org/content/344/6188/1173/suppl/DC1
Materials and Methods
Figs. S1 to S8
References (*41*–*43*)

28 November 2013; accepted 28 April 2014
10.1126/science.1249098

SCHIZOPHRENIA

Specific disruption of thalamic inputs to the auditory cortex in schizophrenia models

Sungkun Chun, Joby J. Westmoreland, Ildar T. Bayazitov, Donnie Eddins, Amar K. Pani, Richard J. Smeyne, Jing Yu, Jay A. Blundon, Stanislav S. Zakharenko*

Auditory hallucinations in schizophrenia are alleviated by antipsychotic agents that inhibit D2 dopamine receptors (Drd2s). The defective neural circuits and mechanisms of their sensitivity to antipsychotics are unknown. We identified a specific disruption of synaptic transmission at thalamocortical glutamatergic projections in the auditory cortex in murine models of schizophrenia-associated 22q11 deletion syndrome (22q11DS). This deficit is caused by an aberrant elevation of Drd2 in the thalamus, which renders 22q11DS thalamocortical projections sensitive to antipsychotics and causes a deficient acoustic startle response similar to that observed in schizophrenic patients. Haploinsufficiency of the microRNA-processing gene *Dgcr8* is responsible for the Drd2 elevation and hypersensitivity of auditory thalamocortical projections to antipsychotics. This suggests that *Dgcr8*-microRNA-Drd2–dependent thalamocortical disruption is a pathogenic event underlying schizophrenia-associated psychosis.

Schizophrenia (SCZ) is one of the most debilitating forms of mental illness (*1*). Positive symptoms of SCZ, including auditory hallucinations, are among the most enigmatic. Antipsychotic agents acting via D2 dopamine receptors (Drd2s) alleviate auditory hallucinations in most patients (*2*, *3*) but do not treat other symptoms (such as cognitive deficits, dampened emotions, and social withdrawal) (*4*). Sensory cortex malfunction has been implicated in hallucinations (*5*, *6*), but which neural circuits become faulty and how they develop selective sensitivity to antipsychotics are unknown.

We tested synaptic transmission at excitatory projections in the auditory cortex (ACx) of *Df(16)1*/+ mice (*7*, *8*), a mouse model of schizophrenia-associated 22q11 deletion syndrome (22q11DS) (*9*) (Fig. 1A). Because positive symptoms emerge during adolescence or early adulthood, we used mature (4- to 5-month-old) mice. We measured evoked AMPA receptor (AMPAR)–mediated excitatory postsynaptic currents (EPSCs) from layer (L) 3/4 pyramidal neurons, the main thalamorecipient neurons in the ACx (*10*), in response to stimulation of thalamocortical (TC) or corticocortical [CC (L3/4-L3/4 or L1-L3/4)] projections in slices containing the auditory thalamus [the ventral medial geniculate nucleus (MGv)], ACx, and hippocampus (Fig. 1, B to E). We also measured synaptic transmission at corticothalamic (CT) projections by recording CT EPSCs in MGv thalamic neurons (Fig. 1F) and at hippocampal CA3-CA1 projections by recording field excitatory postsynaptic potentials (fEPSPs) (Fig. 1G). Only TC projections were deficient in *Df(16)1*/+ mice as compared to wild-type (WT) littermates [30 (WT)/30 (*Df(16)1*/+) neurons] (Fig. 1C and fig. S1), and this deficit occurred in both female and male mice (fig. S2). Synaptic transmission at CC [19 out of 19 (19/19) and 17/16 neurons for L3/4-L3/4 and L1-L3/4, respectively], CT (14/16 neurons), or hippocampal (24/29 slices) projections was normal (Fig. 1, D to G, and fig. S1).

Several findings supported the idea that TC deficiency in *Df(16)1*/+ mice is presynaptic. Two-photon calcium imaging in dendritic spines of L3/4 neurons loaded with the calcium indicator Fluo-5F and cytoplasmic dye Alexa 594 (Fig. 1H) identified functional TC inputs (Fig. 1I). The

Department of Developmental Neurobiology, St. Jude Children's Research Hospital, Memphis, TN 38105, USA.
***Corresponding author. E-mail: stanislav.zakharenko@stjude.org**

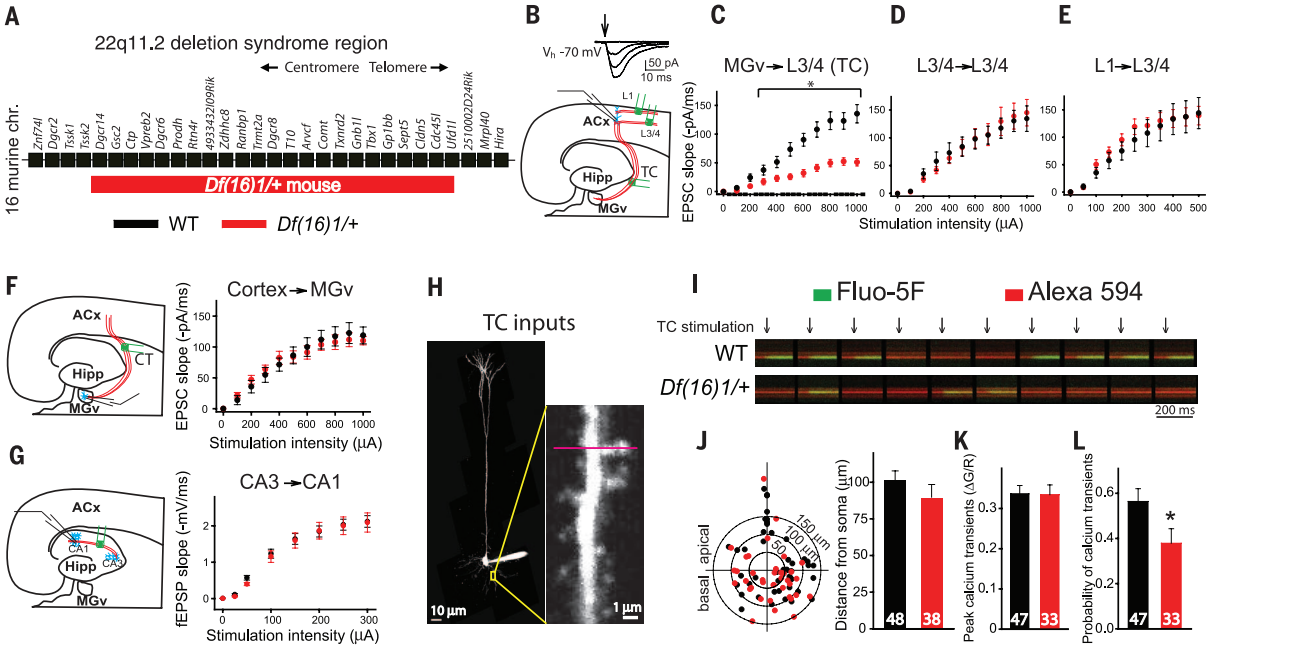

Fig. 1. Specific deficit of TC synaptic transmission to the ACx of 22q11DS mice. (**A**) Map of 22q11DS orthologs in *Df(16)1/+* mice. (**B**) Voltage-clamp recordings in thalamorecipient L3/4 pyramidal neurons. Arrow, electrical stimulation (top). TC slices showing the MGv, hippocampus (Hipp), and ACx (bottom). (**C** to **E**) Input-output relationships between stimulation intensity and EPSCs at TC (MGv-L3/4) (C), L3/4-L3/4 (D), and L1-L3/4 (E) projections. (**F** and **G**) CT EPSC and CA3-CA1 fEPSP recordings (left) and input-output relationship (right). (**H**) L3/4 pyramidal neuron filled with Fluo-5F and Alexa 594 (left) to visualize dendritic spines (right). The red line represents the line scan. (**I**) Calcium transients in a dendritic spine in response to a single TC stimulation (arrows) repeated 10 times (0.1 Hz). (**J**) TC input locations on dendritic trees of L3/4 pyramidal neurons [48 (WT)/38 (*Df(16)1/+*) spines from 17 (WT)/11 (*Df(16)1/+*) neurons] (left); (0;0), soma coordinates. Average distances from soma to TC inputs (right) are shown. (**K** and **L**) Calcium transient amplitudes (K) and probabilities (L) in response to 10 single TC stimulations. The numbers of spines tested are shown inside columns. *$P < 0.05$ [(C) and (L)].

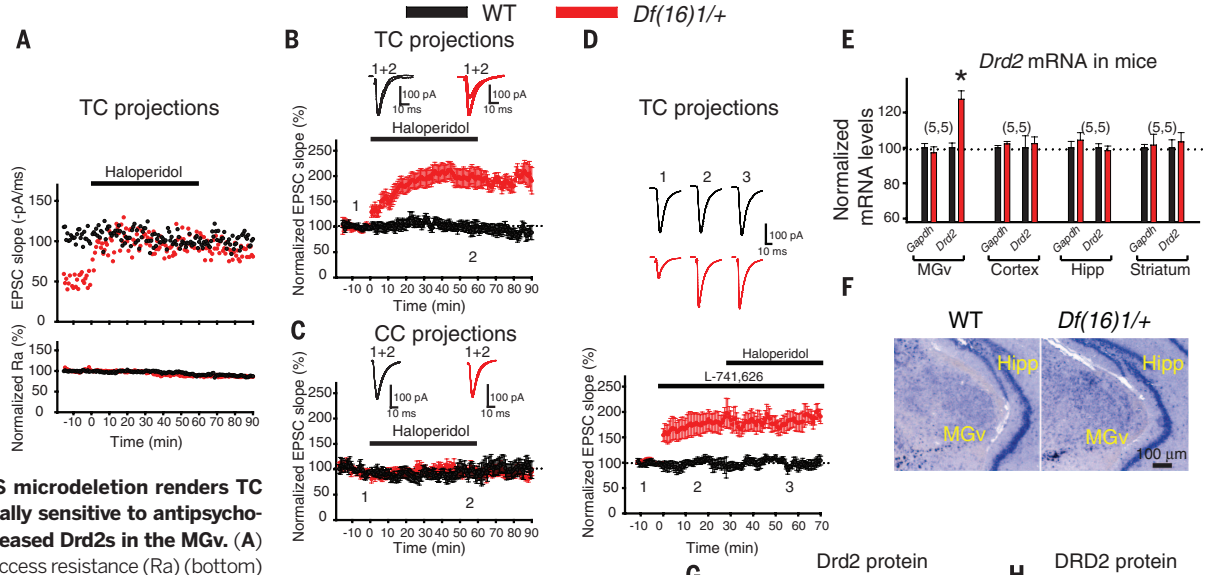

Fig. 2. The 22q11DS microdeletion renders TC projections abnormally sensitive to antipsychotics because of increased Drd2s in the MGv. (**A**) TC EPSCs (top) and access resistance (Ra) (bottom) during repeated TC stimulations (0.05 Hz, 600 μA) before and after haloperidol (1 μM). (**B** and **C**) Mean EPSCs normalized to initial baseline at TC ($P < 0.001$, 16/21 neurons) (B) and L3/4-L3/4 CC projections ($P = 0.75$, 15/14 neurons) (C) before and after haloperidol. (**D**) Normalized TC EPSCs before and after L-741,626 (20 nM) and haloperidol (5/12 neurons). (Insets) Representative EPSC traces. (**E**) Average mRNA levels of *Drd2* normalized to *Gapdh* in different brain regions. (**F**) *Drd2* in situ hybridization. (**G** and **H**) Average Drd2 and DRD2 protein levels normalized to β-actin in mice (G) and the MGv from postmortem tissues of healthy human controls and patients with SCZ (H). Numbers of mice or human samples are shown inside columns or parentheses. *$P < 0.05$ [(E), (G), and (H)].

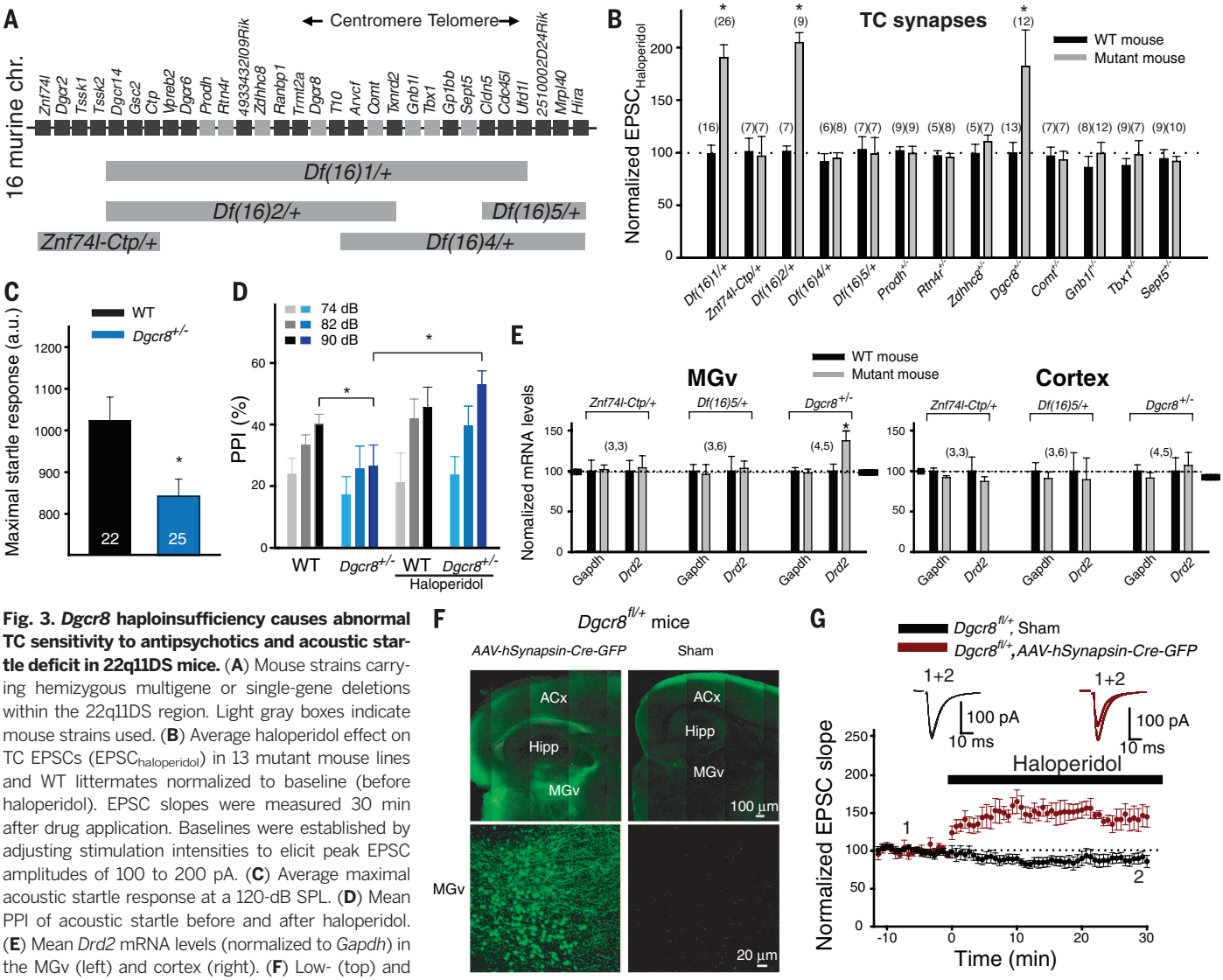

Fig. 3. *Dgcr8* haploinsufficiency causes abnormal TC sensitivity to antipsychotics and acoustic startle deficit in 22q11DS mice. (**A**) Mouse strains carrying hemizygous multigene or single-gene deletions within the 22q11DS region. Light gray boxes indicate mouse strains used. (**B**) Average haloperidol effect on TC EPSCs ($EPSC_{haloperidol}$) in 13 mutant mouse lines and WT littermates normalized to baseline (before haloperidol). EPSC slopes were measured 30 min after drug application. Baselines were established by adjusting stimulation intensities to elicit peak EPSC amplitudes of 100 to 200 pA. (**C**) Average maximal acoustic startle response at a 120-dB SPL. (**D**) Mean PPI of acoustic startle before and after haloperidol. (**E**) Mean *Drd2* mRNA levels (normalized to *Gapdh*) in the MGv (left) and cortex (right). (**F**) Low- (top) and high- (bottom) magnification images of a TC slice from $Dgcr8^{fl/+}$ mice injected with *AAV-hSynapsin-Cre-GFP* (left) or ACSF (sham, right). (**G**) Mean TC EPSCs before and after haloperidol in $Dgcr8^{fl/+}$ mice injected in vivo with *AAV-hSynapsin-Cre-GFP* or sham ($P < 0.05$, 8/6 neurons). Insets show representative TC EPSCs. The dotted line indicates the baseline. Numbers of neurons (B) or mice [(C) and (E)] are shown inside columns or parentheses.*$P < 0.05$.

distribution of thalamic inputs on dendritic trees and the calcium-transient amplitudes were normal (Fig. 1, J and K), but calcium-transient probability was deficient at TC synapses of *Df(16)1/+* mice (Fig. 1L). Paired-pulse depression evoked electrically or optogenetically was reduced at *Df(16)1/+* TC projections (fig. S3). The FM 1-43 assay (*11*) showed slower dye release from TC terminals in mutant mice (fig. S4). Monosynaptic TC *N*-methyl-D-aspartate receptor (NMDAR)–dependent EPSCs were also deficient in *Df(16)1/+* mice (fig. S5). However, the NMDAR/AMPAR ratio was unaffected (fig. S6). Minimal electrical stimulation of the thalamic radiation that typically evoked unitary EPSCs (successes) or no ESPCs (failures) revealed reduced release probability in TC projections of *Df(16)1/+* mice (fig. S7). A synaptic deficiency rather than a decrease in the excitability of thalamic neurons seemed to cause the presynaptic deficit at *Df(16)1/+* TC projections (fig. S8).

The antipsychotics haloperidol (1 µM) and clozapine (40 µM) reversed the synaptic defect of *Df(16)1/+* TC connections (Fig. 2 and fig. S9). Normalized EPSC data revealed that *Df(16)1/+* (but not WT) TC projections are sensitive to antipsychotics (Fig. 2B and fig. S9A). CC projections of both genotypes remained insensitive to the drugs (Fig. 2C and figs. S9B and S10 to S12). The response of mutant TC projections to antipsychotics was dose-dependent (fig. S13). Approximately 85% of mutant TC neurons responded more strongly than WT neurons to antipsychotics (fig. S14). In contrast to the ACx, TC projections in *Df(16)1/+* somatosensory or visual cortices were not sensitive to haloperidol (fig. S15).

The sensitivity of *Df(16)1/+* TC projections to antipsychotics was mediated by Drd2s. The Drd2-specific antagonist L-741,626 (20 nM) enhanced TC EPSCs in *Df(16)1/+* but not WT mice (Fig. 2D). Subsequent application of haloperidol did not induce an additional effect, suggesting that both agents act through Drd2s (Fig. 2D). Drd2 agonist quinpirole (0.5 to 20 µM) did not affect TC or CC EPSCs in WT or *Df(16)1/+* mice (fig. S16). Dopaminergic projections from the ventral tegmental area were present in the thalamic radiation and ACx (fig. S17) and therefore may deliver dopamine to TC projections. We hypothesized that ambient dopamine in the MGv and ACx may activate abnormally upregulated Drd2 in TC projections of *Df(16)1/+* mice. Quantitative real-time polymerase chain reaction (Fig. 2E) and in situ hybridization (Fig. 2F and fig. S18) revealed an increase in *Drd2* transcript levels in the *Df(16)1/+* MGv. Splice variants of *Drd2* (*D2Short* and *D2Long*) (fig. S19) and Drd2 protein levels (Fig. 2G) were comparably increased in the *Df(16)1/+* MGv. Transcript and protein levels

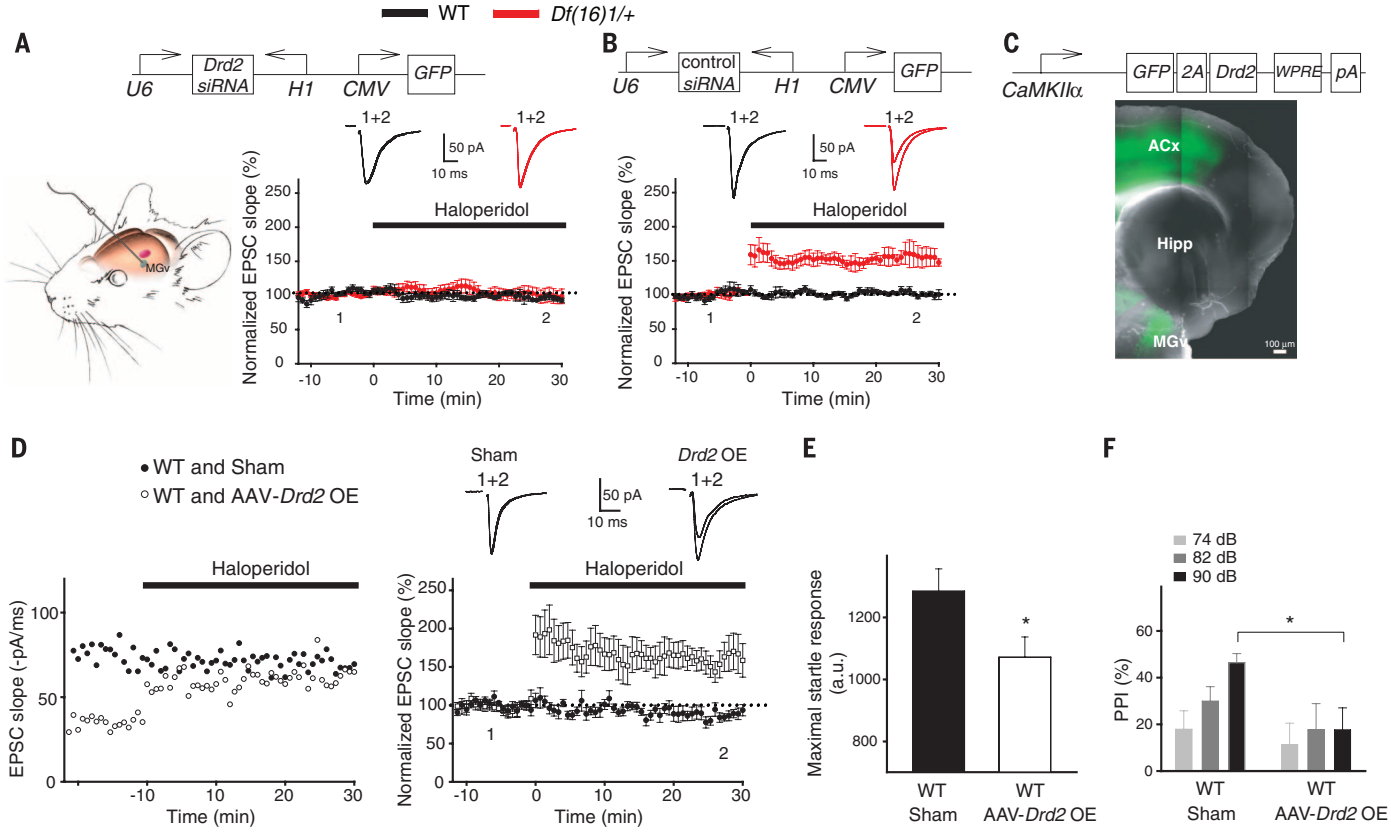

Fig. 4. Aberrant Drd2 elevation in MGv neurons is necessary and sufficient to render TC projections sensitive to antipsychotics. (**A** and **B**) *Drd2* [(A), top] and control [(B), top] siRNA viruses. In vivo MGv viral injection [(A), bottom left]. Mean TC EPSCs before and after haloperidol in mice injected with *Drd2* siRNA [(A), bottom right] ($P = 0.67$, 9/11 neurons) or control siRNA viruses (B, bottom) ($P = 0.016$, 7/9 neurons) are shown. (**C**) Composition of the *Drd2*-OE virus [woodchuck hepatitis posttranscriptional regulatory element (*WPRE*), polyA signal (*pA*)] (top) and TC slice showing green fluorescent protein (*GFP*) in MGv neurons (bottom). (**D**) Representative TC EPSCs (left) and mean normalized TC EPSCs (right) before and after haloperidol from WT mice injected with *Drd2*-OE or sham ($P < 0.05$, 7/9 neurons). (**E** and **F**) Acoustic startle response (E) at a 120-dB SPL and PPI (F) in WT mice injected with *Drd2*-OE or sham (10 mice each) into the MGv, $^*P < 0.05$. Dotted lines, baseline; insets, representative TC EPSCs.

increased in the thalamus but not the cortex, hippocampus, and striatum (Fig. 2, E and G). However, total dopamine levels in all regions assayed were comparable between both genotypes (fig. S20). In postmortem human tissues (Fig. 2H and table S1), DRD2 protein levels in the MGv were higher in SCZ patients than in healthy controls ($P < 0.001$, 13 patients per group).

We next screened 12 mouse strains carrying hemizygous deletions of gene clusters or individual genes within the microdeletion for haloperidol sensitivity (Fig. 3A). We measured TC EPSCs before and after haloperidol application in mutants and WT littermates. In addition to *Df(16)1/+*, only *Df(16)2/+* and *Dgcr8*$^{+/-}$ mice responded to haloperidol (Fig. 3B). The microRNA-processing gene *Dgcr8* is encoded within the *Df(16)2* region (Fig. 3A). Like *Df(16)1/+*, approximately 80% of *Dgcr8*$^{+/-}$ neurons responded more strongly than WT neurons to the antipsychotics (figs. S21 and S22), implying an impaired flow of acoustic information in *Dgcr8*$^{+/-}$ mice. The acoustic startle response was lower in mature *Dgcr8*$^{+/-}$ mice than in WT littermates (22/25 mice, $P < 0.05$) (Fig. 3C). This deficit may affect prepulse inhibition (PPI) of acoustic startle, a characteristic feature of SCZ in animal models and human patients. *Dgcr8*$^{+/-}$ mice were deficient in PPI [24/29 mice, $P < 0.05$ at a 90-dB sound pressure level (SPL)] (Fig. 3D), and this deficit was rescued by haloperidol ($P < 0.05$ at a 90-dB SPL) (Fig. 3D).

Consistent with the notion that *Dgcr8* haploinsufficiency underlies the sensitivity of TC projections to antipsychotics in 22q11DS, *Drd2* mRNA levels were found to be increased in the MGv but not the cortex of *Dgcr8*$^{+/-}$ mice (Fig. 3E). *Znf74l-Ctp/+* and *Df(16)5/+* microdeletions, which do not include *Dgcr8*, produced no increase in *Drd2* (Fig. 3E), but *Df(16)2/+* mice carrying a *Dgcr8*-containing microdeletion did (fig. S23).

Conditional *Dgcr8* hemizygous deletion in MGv neurons (Fig. 3F) rendered TC projections sensitive to antipsychotics (Fig. 3G), indicating that MGv-specific reduction in *Dgcr8* underlies TC deficiency in 22q11DS mice.

To test whether Drd2 elevation causes TC deficiency, we knocked down *Drd2* in MGv neurons (Fig. 4A and fig. S24A). *Drd2* small interfering RNA (siRNA) but not scrambled (control) siRNA decreased *Drd2* levels in the MGv (fig. S24B) and eliminated the sensitivity of mutant TC projections to antipsychotics (Fig. 4, A and B). Drd2 overexpression in MGv excitatory neurons (Fig. 4C) made WT TC projections sensitive to haloperidol (Fig. 4D) and caused deficits in acoustic startle and PPI in WT mice (Fig. 4, E and F).

Thus, we have identified that an SCZ-associated microdeletion up-regulates Drd2 in thalamic neurons and disrupts glutamatergic synaptic transmission at TC projections to the ACx, and this is caused by haploinsufficiency of *Dgcr8*. This mechanism integrates several competing SCZ models such as dopamine hyperfunction theory (*2*), glutamatergic hypofunction theory (*12*), TC disconnectivity theory (*13*), and TC loop dysfunction models (*14*). Our results indicate disturbances in the *Dgcr8*-microRNA-Drd2 pathway in thalamic projections to the ACx as a pathogenic mechanism that alters the normal flow of auditory information and thereby contributes to positive symptoms of SCZ.

REFERENCES AND NOTES

1. T. R. Insel, *Nature* **468**, 187–193 (2010).
2. A. Carlsson, *Neuropsychopharmacology* **1**, 179–186 (1988).
3. S. H. Snyder, *Philos. Trans. R. Soc. London Ser. B* **354**, 1985–1994 (1999).
4. S. Miyamoto, N. Miyake, L. F. Jarskog, W. W. Fleischhacker, J. A. Lieberman, *Mol. Psychiatry* **17**, 1206–1227 (2012).
5. T. Dierks *et al.*, *Neuron* **22**, 615–621 (1999).

6. D. Hubl, T. Koenig, W. K. Strik, L. M. Garcia, T. Dierks, *Br. J. Psychiatry* **190**, 57–62 (2007).
7. E. A. Lindsay *et al*., *Nature* **401**, 379–383 (1999).
8. E. A. Lindsay *et al*., *Nature* **410**, 97–101 (2001).
9. 22q11DS is caused by the hemizygous deletion of a 1.5- to 3-megabase region of the q arm of human chromosome 22, and SCZ develops in approximately 30% of patients with 22q11DS. *Df(16)1/+* mice carry a hemizygous deletion of 23 genes in the syntenic region of chromosome 16.
10. P. H. Smith, L. C. Populin, *J. Comp. Neurol.* **436**, 508–519 (2001).
11. S. S. Zakharenko, L. Zablow, S. A. Siegelbaum, *Nat. Neurosci.* **4**, 711–717 (2001).
12. J. T. Coyle, *Harv. Rev. Psychiatry* **3**, 241–253 (1996).
13. N. D. Woodward, H. Karbasforoushan, S. Heckers, *Am. J. Psychiatry* **169**, 1092–1099 (2012).
14. R. P. Behrendt, *Conscious. Cogn.* **12**, 413–451 (2003).

ACKNOWLEDGMENTS

This work was supported, in part, by NIH grants R01 MH097742, R01 MH095810, and R01 DC012833 and the American Lebanese Syrian Associated Charities. We thank E. Illingworth, P. Scambler, A. Wynshaw-Boris, J. Gogos, S. Strittmatter, B. Morrow, and E. Fuchs for providing mutant mice; A. Lessard and the Maryland Brain Collection for providing postmortem human brain samples; K. J. Sample and P. Devaraju for technical assistance; and St. Jude Children's Research Hospital, University of Tennessee, University of North Carolina, and University of Pennsylvania Vector Cores for producing adeno-associated viruses and lentiviruses.

SUPPLEMENTARY MATERIALS

www.sciencemag.org/content/344/6188/1178/suppl/DC1
Materials and Methods
Figs. S1 to S24
Table S1
References (*15*–*20*)

25 March 2014; accepted 14 May 2014
10.1126/science.1253895

NEURODEVELOPMENT

Cell-intrinsic requirement of Dscam1 isoform diversity for axon collateral formation

Haihuai He,[1,2,3]* Yoshiaki Kise,[1,2]* Azadeh Izadifar,[1,2] Olivier Urwyler,[1,2] Derya Ayaz,[1,2]† Akhila Parthasarthy,[3] Bing Yan,[1,2] Maria-Luise Erfurth,[1,2,4] Dan Dascenco,[1,2] Dietmar Schmucker[1,2]‡

The isoform diversity of the *Drosophila* Dscam1 receptor is important for neuronal self-recognition and self-avoidance. A canonical model suggests that homophilic binding of identical Dscam1 receptor isoforms on sister dendrites ensures self-avoidance even when only a single isoform is expressed. We detected a cell-intrinsic function of Dscam1 that requires the coexpression of multiple isoforms. Manipulation of the Dscam1 isoform pool in single neurons caused severe disruption of collateral formation of mechanosensory axons. Changes in isoform abundance led to dominant dosage-sensitive inhibition of branching. We propose that the ratio of matching to nonmatching isoforms within a cell influences the Dscam1-mediated signaling strength, which in turn controls axon growth and growth cone sprouting. Cell-intrinsic use of surface receptor diversity may be of general importance in regulating axonal branching during brain wiring.

Several classes of neuronal cell surface receptors exhibit an exceptional degree of protein diversity and have been implicated in important aspects of neuronal differentiation (*1*–*5*). Evidence for the importance of isoform diversity during development has been provided for the *Drosophila* Down syndrome cell adhesion molecule (Dscam1) and the mouse clustered protocadherins (PCDHs) (*6*–*14*). The *Dscam1* gene uses combinatorial alternative splicing to generate tens of thousands of different receptor isoforms, whereas the clustered PCDHs rely on combinatorial oligomerization to provide a huge diversification of their binding specificities (*2*, *7*, *9*, *11*). The isoform diversity is thought to provide neurons with distinct "surface tags," thereby endowing them with unique molecular identities. Such complex molecular recognition mechanisms are particularly important for the development of highly branched neurite compartments.

Many neuronal circuits depend on the presence of highly branched axons or dendrites, which serve to increase either the wiring complexity or the size of the input/output fields. The development of branched dendritic fields requires a dedicated mechanism—often referred to as self-avoidance—that ensures correct spacing between sister neurites and prevents hypo- or hyperinnervation (*7*). For Dscam1 it has been shown that isoform-specific homophilic binding on the surface of sister dendrites provides the molecular recognition mechanism that underlies neurite repulsion and self-avoidance (*12*–*14*). This molecular model of self-avoidance has also been proposed for the vertebrate PCDH gamma receptors (*10*).

This model, which we refer to as the canonical model of Dscam1/PCDH function, states that isoform-specific homophilic receptor binding on the surface of sister dendrites initiates neurite repulsion, and that the expression of a single Dscam1 isoform per neuron is sufficient for Dscam1 function (*12*–*15*). The question of whether this canonical role provides the mechanistic basis of all Dscam1 functions is still open to debate (*3*, *7*, *9*). Addressing this point, we found evidence for a strictly cell-intrinsic requirement of multiple diverse Dscam1 isoforms and describe a function of isoform diversity specifically required for the patterning of complex axonal arborizations.

To examine the role of Dscam1 diversity, we generated bacterial artificial chromosome (BAC)–based conditional alleles (*16*) that express Dscam1 protein at endogenous levels and allow for the manipulation of Dscam1 diversity in a spatially and temporally specific manner (Fig. 1A) (*17*). We found that the *[Dscam1]EX6.1-FRT* allele recapitulates all known neuronal wiring functions of Dscam1 and is functionally equivalent to the endogenous *Dscam1* (Fig. 1, fig. S1, and table S1). We analyzed thoracic mechanosensory (MS) neurons, which innervate the macrochaetae of adult flies and show a stereotypic axonal branching pattern in the ventral nerve cord (VNC) (*3*) (Fig. 1B). The loss of *Dscam1* in MS neurons causes severe MS axon growth and branch patterning defects (*3*) (Fig. 1C). However, replacing the endogenous *Dscam1* locus with the BAC-based *[Dscam1]EX6.1-FRT* allele rescued all mutant defects (fig. S1).

In sharp contrast to the *[Dscam1]EX6.1-FRT* allele, the *[Dscam1]EX6.1-Flpd* allele lacking all but one of the exon 6 variants (Fig. 1A) did not restore the axon collateral formation (Fig. 1, D and E). Often only an ipsilateral primary axon shaft was formed (Fig. 1E), but collateral branches were missing (78%, $n = 37$). In some cases, primary branches were formed but lacked higher-order branches and varicosities (fig. S2) (22%, $n = 37$). Because similar branching defects have been observed in experiments where exon 9 diversity was lacking in whole flies (*8*), we conclude that any substantial and global reduction in Dscam1 isoform diversity causes a loss of MS axon collaterals.

The use of BAC-based *Dscam1* alleles allowed us to combine multiple engineered and endogenous *Dscam1* alleles and revealed a striking dominant and dosage-dependent influence of Dscam1 diversity on axonal branching (Fig. 1, F to I). A single copy of *[Dscam1]EX6.1-Flpd* in a wild-type background dominantly caused a specific lack of a primary anterior ipsilateral branch (86%) (Fig. 1H). When two copies of *[Dscam1]EX6.1-Flpd* were added, the dominant phenotype was enhanced such that additional primary branches were missing in 45% of the

[1]Neuronal Wiring Laboratory, Vlaams Instituut voor Biotechnologie (VIB) Vesalius Research Center, 3000 Leuven, Belgium. [2]Department of Oncology, School of Medicine, University of Leuven, 3000 Leuven, Belgium. [3]Department of Cancer Biology, Dana-Farber Cancer Institute, Boston, MA 02215, USA. [4]Institute of Biochemistry, Christian-Albrechts-University of Kiel, 24118 Kiel, Germany.
*These authors contributed equally to this work. †Present address: Laboratory of Ion Channel Research, University of Leuven, 3000 Leuven, Belgium. **‡Corresponding author. E-mail: dietmar.schmucker@vib-kuleuven.be**